

# Expanding Polyhedral Universe in Regge Calculus

REN TSUDA<sup>1</sup> AND TAKANORI FUJIWARA<sup>2</sup>

<sup>1</sup> *Graduate School of Science and Engineering, Ibaraki University, Mito 310-8512, Japan*

<sup>2</sup> *Department of Physics, Ibaraki University, Mito 310-8512, Japan*

## Abstract

The closed Friedmann–Lemaître–Robertson–Walker (FLRW) universe of Einstein gravity with positive cosmological constant in three dimensions is investigated by using the Collins–Williams formalism in Regge calculus. A spherical Cauchy surface is replaced with regular polyhedrons. The Regge equations are reduced to differential equations in the continuum time limit. Numerical solutions to the Regge equations approximate well the continuum FLRW universe during the era of small edge length. The deviation from the continuum solution becomes larger and larger with time. Unlike the continuum universe, the polyhedral universe expands to infinite within finite time. To remedy the shortcoming of the model universe we introduce geodesic domes and pseudo-regular polyhedrons. It is shown that the pseudo-regular polyhedron model can approximate well the results of the Regge calculus for the geodesic domes. The pseudo-regular polyhedron model approaches the continuum solution in the infinite frequency limit.

# 1 Introduction

Regge calculus was proposed to formulate Einstein's general relativity on piecewise linear manifolds [1, 2]. It provides a coordinate-free lattice formulation of gravitation and has been used in investigations of classical as well as quantum gravity. Like QCD, the lattice theoretical approach provides a powerful framework in nonperturbative studies of quantum gravity [3]. However, before moving to detailed quantum study, the formalism at the classical level should be investigated. Any lattice regularized theory should reproduce the basic results of the corresponding continuum theory. Taking the classical continuum limit is relatively easy in the case of lattice gauge theories. The reason for this is obvious: In lattice gauge theory, space-time itself is not dynamical. We usually consider a hypercubic regular lattice for the space-time. Dynamical variables sit on sites for matter fields and on links for gauge fields. Classical lattice actions are written in manifestly gauge-invariant form by using plaquette variables and covariant differences, which have obvious classical counterparts. The point is that in the lattice gauge it is easy, at least classically, to investigate how the theories behave under changes of lattice size and lattice spacing.

In Regge calculus, the space-time is replaced with a piecewise linear manifold, which is composed of a set of simplices. The basic variables are the edge lengths. As in general relativity, the space-time itself should be considered dynamical. We do not know, however, the space-time to be investigated precisely from the beginning. To prepare the Regge action we must assume the topology of the space-time. For a given topology we can triangulate the space-time and write the Regge action. In general there is no natural choice of the piecewise linear manifold. Furthermore, the Regge action is written in coordinate-free form. It is a highly complicated function of the edge length depending heavily on the triangulations of the space-time. This makes investigations of how the theory behaves with respect to refinement of the triangulation much more involved than the lattice gauge theory.

In this note we investigate the Friedmann–Lemaître–Robertson–Walker (FLRW) universe of three-dimensional Einstein gravity with positive cosmological constant in Regge calculus by taking polyhedrons as the Cauchy surface. We compare the solutions between regular polyhedrons, and propose a generalization of the Regge equations beyond them; this makes the numerical analysis much easier than the orthodox Regge calculus.

The continuum action is given by

$$S = \frac{1}{16\pi} \int d^3x \sqrt{-g} (R - 2\Lambda). \quad (1.1)$$

It is well known in three dimensions that the vacuum Einstein equation leads to a flat space-time without the cosmological term. In the case of a negative cosmological constant the theory admits a black hole solution [4, 5] and has been investigated within the context of conformal field theory [6]. As in four dimensions, the Einstein equations have an evolving

universe as a solution for the FLRW metric ansatz

$$ds^2 = -dt^2 + a(t)^2 \left( \frac{dr^2}{1 - kr^2} + r^2 d\varphi^2 \right), \quad (1.2)$$

where  $a(t)$  is the so-called scale factor. It is subject to the Friedmann equations

$$\dot{a}^2 = \Lambda a^2 - k, \quad \ddot{a} = \Lambda a. \quad (1.3)$$

The curvature parameter  $k = 1, 0, -1$  corresponds to space being spherical, Euclidean, or hyperspherical, respectively. Of these, our concern is the spherical universe, which can be approximated by a convex polyhedron of finite volume. Regge calculus has been applied to the four-dimensional closed FLRW universe by Collins and Williams [7]. They considered regular polytopes as the Cauchy surfaces of the discrete FLRW universe and used, instead of simplices, truncated world-tubes evolving from one Cauchy surface to the next as the building blocks of piecewise linear space-time. Their method, called the Collins–Williams (CW) formalism, is based on the idea of the  $3 + 1$  decomposition of space-time and plays a similar role to the well-known Arnowitt–Deser–Misner (ADM) formalism [8]. Recently, Liu and Williams have extensively studied the discrete FLRW universe [9, 10]. They found that a universe with regular polytopes as the Cauchy surfaces can reproduce the continuum FLRW universe to a certain degree of precision. Their solutions agree reasonably well with the continuum when the size of the universe is small, whereas the deviations from the exact results become large for a large universe because of the finite edge length. Since the Regge action depends heavily on the choice of polytopes to approximate the Cauchy surface, it seems to be hard to take the continuum limit while keeping the action simple. This motivates us to investigate a simpler but less realistic three-dimensional model.

In four dimensions there are six types of regular polytopes. Restricting to those obtained by tessellating the three-dimensional sphere by regular tetrahedrons, there are only three, with 5, 16, and 600 cells [11]. The foregoing investigations are mainly restricted to these regular polytopes. The Regge equations, however, are still very complicated. As we shall show, the situation becomes much simpler in three dimensions, where every geometric calculation can be done without complications coming from higher dimensions. This is the reason why we consider three dimensions, where the spherical Cauchy surfaces are replaced by regular polyhedrons. There are five types of polyhedrons. We treat them in a unified way and give generic expressions for the Regge equations that are convenient to analyze beyond the regular polyhedrons.

Let us briefly summarize the essence of Regge calculus. In Regge calculus, an analog of the Einstein–Hilbert action is given by the Regge action [12]

$$S_{\text{Regge}} = \frac{1}{8\pi} \left( \sum_{i \in \{\text{hinges}\}} \varepsilon_i A_i - \Lambda \sum_{i \in \{\text{blocks}\}} V_i \right), \quad (1.4)$$

where  $A_i$  is the volume of a hinge,  $\varepsilon_i$  the deficit angle around the hinge  $A_i$ , and  $V_i$  the volume of a building block of the piecewise linear manifold. In three dimensions the hinges are the links, or equivalently the edges of the 3-simplices, and  $A_i$  is nothing but the edge length  $l_i$ . Regge's original derivation is concerned with a simplicial lattice, so that it describes the gravity as simplicial geometry. This formalism can easily be generalized to arbitrary lattice geometries. We can fully triangulate the non-simplicial flat blocks by adding extra hinges with vanishing deficit angles [9] without affecting the Regge action.

The fundamental variables in Regge calculus are the edge lengths  $l_i$ . Varying the Regge action with respect to  $l_i$ , we obtain the Regge equations

$$\sum_{i \in \{\text{hinges}\}} \varepsilon_i \frac{\partial A_i}{\partial l_j} - \Lambda \sum_{i \in \{\text{blocks}\}} \frac{\partial V_i}{\partial l_j} = 0. \quad (1.5)$$

Note that there is no need to carry out the variation of the deficit angles owing to the Schläfli identity [13, 14]

$$\sum_{i \in \{\text{hinges}\}} A_i \frac{\partial \varepsilon_i}{\partial l_j} = 0. \quad (1.6)$$

In three dimensions, the Regge equations simply relate the deficit angle around an edge to the total rate of variation of the volumes having the edge in common with respect to the edge length. In particular, the space-time becomes flat in the absence of the cosmological term, as it should be.

This paper is organized as follows: In the next section we set up the regular polyhedral universe in the CW formalism and introduce the Regge action. Derivation of the Regge equations is given in Sect. 3. In the continuum time limit the Regge equations are reduced to differential equations. Applying the Wick rotation, we arrive at the Regge calculus analog of the Friedmann equations, describing the evolution of the polyhedral universe. This is done in Sect. 4. In Sect. 5 we solve the differential Regge equation numerically and compare the scale factors of the polyhedral universe with the continuum solution. To obtain better approximations we introduce geodesic domes as the Cauchy surface. In Sect. 6 we propose a pseudo-regular polyhedral universe with a fractional Schläfli symbol as a substitute for the geodesic dome universe and show that the features of the geodesic dome universe can be described well by the pseudo-regular polyhedron model. It is also argued that the continuum solution can be recovered in the infinite frequency limit. Section 7 is devoted to summary and discussions. In Appendix A, the Regge calculus for the first two, simplest, geodesic domes is described.

	Tetrahedron	Cube	Octahedron	Dodecahedron	Icosahedron
$N_0$	4	8	6	20	12
$N_1$	6	12	12	30	30
$N_2$	4	6	8	12	20
$\{p, q\}$	$\{3, 3\}$	$\{4, 3\}$	$\{3, 4\}$	$\{5, 3\}$	$\{3, 5\}$

Table 1: The five regular polyhedrons in three dimensions.

## 2 Regge action for a regular polyhedral universe

The FLRW metric (1.2) describes an expanding or contracting universe with a maximally symmetric space as the Cauchy surface. Surfaces of maximally symmetric compact space are spheres, geometrically characterized by the radius  $a(t)$ , the scale factor in cosmology. In this paper we will be concerned with the Regge calculus of the closed FLRW universe in three dimensions, which describes an evolution of a two-dimensional sphere. Following the CW formalism, we replace the spherical Cauchy surfaces by regular polyhedrons. The fundamental building blocks of space-time are world-tubes of truncated pyramids or frustums, as depicted in Fig. 1. In this section we restrict ourselves to regular polyhedrons as the Cauchy surfaces. Then every edge has equal length in each Cauchy surface, and so does any strut between two adjacent Cauchy surfaces. Evolution of the universe can be seen by focusing our attention only on expanding or shrinking of a face of the polyhedron. This considerably reduces the number of dynamical variables.

It is well known that there are only five types of regular polyhedron: tetrahedron, cube, octahedron, dodecahedron, and icosahedron. Let us denote the numbers of vertices, edges, and faces of a polyhedron by  $N_0$ ,  $N_1$ , and  $N_2$ , respectively. Then they are constrained by Euler's polyhedron formula,

$$N_0 - N_1 + N_2 = 2. \quad (2.1)$$

A regular polyhedron is specified by the Schläfli symbol  $\{p, q\}$ , where  $p$  is the number of sides of each face and  $q$  the number of faces meeting at each vertex. This gives rise to the further constraints  $N_0 = 2N_1/q$  and  $N_1 = pN_2/2$ . These, together with Eq. (2.1), completely determine  $N_{0,1,2}$ . In Table 1 we summarize the properties of regular polyhedrons for the reader's reference.

The fundamental blocks of space-time in the Regge calculus are frustums with  $p$ -sided regular polygons as the upper and lower faces and  $p$  isosceles trapezoids as the lateral faces, as depicted in Fig. 1. We assume that the upper face of a frustum lies in a time-slice, so does the lower one. The whole space-time is then obtained by gluing such frustums face by face without a break. There are only two types of hinges in this piecewise linear manifold. One type of hinge is the edges of regular polyhedrons. We denote by  $l_i$  the length of the

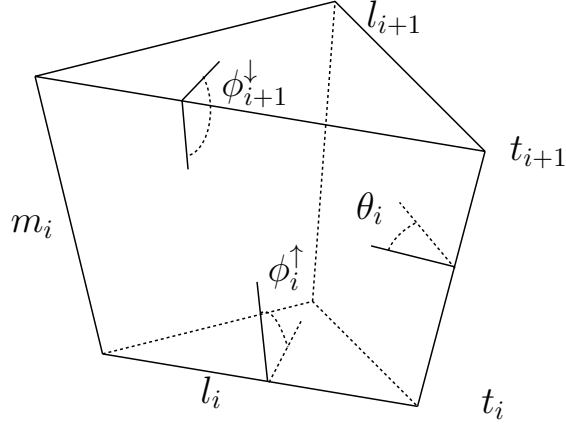


Figure 1: The  $i$ th frustum as the fundamental building block of a polyhedral universe for  $p = 3$ : Each face of the regular polygon with edge length  $l_i$  at time  $t_i$  expands to the upper one with  $l_{i+1}$  at  $t_{i+1}$ .

edges on the  $i$ th Cauchy surface at time  $t_i$ . The other type is the struts between consecutive Cauchy surfaces. We denote by  $m_i$  the length of the struts between the Cauchy surfaces at  $t_i$  and  $t_{i+1}$ . Thus, the Regge action (1.4) can be written as

$$S_{\text{Regge}} = \frac{1}{8\pi} \sum_i (N_0 m_i \varepsilon_i^{(s)} + N_1 l_i \varepsilon_i^{(e)} - N_2 \Lambda V_i), \quad (2.2)$$

where  $\varepsilon_i^{(s)}$  and  $\varepsilon_i^{(e)}$  stand for the deficit angles around the strut and edge, respectively, and  $V_i$  is the world-volume of the frustum. To avoid subtleties in defining lengths and angles, we assume for the time being the metric in each building block to be flat Euclidean, where geometric objects such as lengths and angles are obvious. The equations of motion in Lorentzian geometry can be achieved by the Wick rotation.

### 3 Regge equations

The fundamental variables in Regge calculus are the lengths of the edges  $l_i$  and those of the struts  $m_i$ . The Regge equations can be obtained by applying the variational principle to the action (2.2). Then, Eq. (1.5) can be written simply as

$$\varepsilon_i^{(s)} = \frac{q}{p} \Lambda \frac{\partial V_i}{\partial m_i}, \quad (3.1)$$

$$\varepsilon_i^{(e)} = \frac{2}{p} \Lambda \left( \frac{\partial V_i}{\partial l_i} + \frac{\partial V_{i-1}}{\partial l_i} \right). \quad (3.2)$$

Note that the edge  $l_i$  belongs to both  $V_i$  and  $V_{i-1}$ . In the context of the ADM formalism, the first corresponds to the Hamiltonian constraint and the second to the evolution equation, respectively.

The volume and deficit angles can be expressed in terms of  $l$ 's and  $m$ 's. Since the inside of a frustum is flat Euclidean, we can compute the volumes and angles by standard geometric calculations. The volume of the  $i$ th frustum is given by

$$V_i = \frac{p}{12}(l_{i+1}^2 + l_{i+1}l_i + l_i^2)\sqrt{m_i^2 - \frac{1}{4}\delta l_i^2 \csc^2 \frac{\pi}{p} \cot \frac{\pi}{p}}, \quad (3.3)$$

where we have introduced the variation of edge length  $\delta l_i = l_{i+1} - l_i$ .

The deficit angle around a strut can be found by noting the fact that there are  $q$  frustums having the strut in common. Then,  $\varepsilon_i^{(s)}$  can be expressed as

$$\varepsilon_i^{(s)} = 2\pi - q\theta_i, \quad (3.4)$$

where  $\theta_i$  is the dihedral angle between two adjacent lateral trapezoids. It is explicitly given by

$$\theta_i = \arccos \left( -\frac{4m_i^2 \cos \frac{2\pi}{p} + \delta l_i^2}{4m_i^2 - \delta l_i^2} \right); \quad (3.5)$$

see Fig. 1.

To find the deficit angle around the edge  $l_i$  we must take account of four frustums having the edge in common, two  $V_i$  in the future side and two  $V_{i-1}$  in the past side. Let  $\phi_i^\uparrow$  be the dihedral angle between the base regular polygon and a lateral trapezoid in the frustum  $V_i$ . Similarly, we denote by  $\phi_i^\downarrow$  the dihedral angle between the top regular polygon and a lateral face in  $V_{i-1}$  [9, 10]. As is easily seen in Fig. 1, the dihedral angles are constrained by  $\phi_i^\uparrow + \phi_{i+1}^\downarrow = \pi$ . Then, the deficit angle  $\varepsilon_i^{(e)}$  can be written as

$$\varepsilon_i^{(e)} = 2\pi - 2(\phi_i^\uparrow + \phi_i^\downarrow) = 2\delta\phi_i^\downarrow, \quad (3.6)$$

where we have introduced  $\delta\phi_i^\downarrow = \phi_{i+1}^\downarrow - \phi_i^\downarrow$ . In terms of the lengths of edges and struts, the dihedral angle  $\phi_i^\downarrow$  can be expressed as

$$\phi_i^\downarrow = \arccos \frac{\delta l_{i-1} \cot \frac{\pi}{p}}{\sqrt{4m_{i-1}^2 - \delta l_{i-1}^2}}. \quad (3.7)$$

Inserting these expressions for the deficit angles and volume element into the Regge equations

(3.1) and (3.2), we obtain a set of recurrence relations:

$$2\pi - q \arccos \left( -\frac{4m_i^2 \cos \frac{2\pi}{p} + \delta l_i^2}{4m_i^2 - \delta l_i^2} \right) = \frac{q\Lambda}{12} \frac{(l_{i+1}^2 + l_{i+1}l_i + l_i^2)m_i}{\sqrt{m_i^2 - \frac{1}{4}\delta l_i^2 \csc^2 \frac{\pi}{p}}} \cot \frac{\pi}{p}, \quad (3.8)$$

$$\begin{aligned} \arccos \frac{\delta l_i \cot \frac{\pi}{p}}{\sqrt{4m_i^2 - \delta l_i^2}} - \arccos \frac{\delta l_{i-1} \cot \frac{\pi}{p}}{\sqrt{4m_{i-1}^2 - \delta l_{i-1}^2}} &= \frac{\Lambda}{12} \left[ \frac{(l_{i+1} + 2l_i)m_i^2 + \frac{3}{4}l_i^2 \delta l_i \csc^2 \frac{\pi}{p}}{\sqrt{m_i^2 - \frac{1}{4}\delta l_i^2 \csc^2 \frac{\pi}{p}}} \right. \\ &\quad \left. + \frac{(2l_i + l_{i-1})m_{i-1}^2 - \frac{3}{4}l_i^2 \delta l_{i-1} \csc^2 \frac{\pi}{p}}{\sqrt{m_{i-1}^2 - \frac{1}{4}\delta l_{i-1}^2 \csc^2 \frac{\pi}{p}}} \right] \cot \frac{\pi}{p}. \end{aligned} \quad (3.9)$$

As a consistency check, it is straightforward to see that these admit flat metric solutions for  $\{p, q\} = \{3, 6\}$ ,  $\{4, 4\}$ , and  $\{6, 3\}$  in the absence of the cosmological term.

## 4 Continuum time limit

The nonlinear recurrence relations (3.8) and (3.9) are written only in terms of geometrical data, the edge and strut lengths  $l_i$  and  $m_i$ . To obtain an insight into the evolution of the space-time we first note the relation between the strut length  $m_i$  and the Euclidean time elapsed,  $\delta t_i = t_{i+1} - t_i$ . In Refs. [9, 10], the time axis is chosen to be orthogonal to the Cauchy surface. For regular polyhedrons this works well. However, it does not work so well for general polyhedrons. To see this, let us consider two adjacent building blocks with equal height. If their base polygons are not congruent, two struts to be identified in gluing the building blocks would have different lengths. In the present polyhedral universe the spatial coordinates of each vertex are kept constant during the expansion. If we choose as  $t_i$  the proper time of a clock expanding with a vertex of the polyhedral Cauchy surface, the strut length is given by

$$m_i = \delta t_i. \quad (4.1)$$

This can be applied to any polyhedron.

We assume, for simplicity, all the time intervals  $\delta t_i$  to be equal and then take the continuum time limit  $\delta t_i \rightarrow dt$ . We can regard the edge length as a smooth function of time  $l_i \rightarrow l(t)$ , and

$$\delta l_i = \frac{\delta l_i}{\delta t_i} \delta t_i \rightarrow \dot{l} dt, \quad (4.2)$$

where  $\dot{l} = dl/dt$ . It is straightforward to compute the continuum time limit of Eqs. (3.8)



and (3.9). We find:

$$2\pi - q \arccos \frac{\dot{l}^2 + 4 \cos \frac{2\pi}{p}}{\dot{l}^2 - 4} = \frac{q\Lambda}{2} \frac{l^2 \cos \frac{\pi}{p}}{\sqrt{4 \sin^2 \frac{\pi}{p} - \dot{l}^2}}, \quad (4.3)$$

$$\frac{\ddot{l}}{4 - \dot{l}^2} = -\frac{\Lambda}{4} l \left[ 1 + \frac{l\ddot{l}}{2(4 \sin^2 \frac{\pi}{p} - \dot{l}^2)} \right]. \quad (4.4)$$

Since we have fixed the strut lengths as mentioned above, they disappear from the Regge equations. One can easily verify that these are consistent each other. In other words, the Hamiltonian constraint can be obtained as the first integral of the evolution equation for the initial conditions [10]:

$$l(0) = l_0 = \sqrt{\frac{4\pi}{\Lambda} \left( \frac{2}{p} + \frac{2}{q} - 1 \right) \tan \frac{\pi}{p}}, \quad \dot{l}(0) = 0. \quad (4.5)$$

The cosmological constant must be positive for regular polyhedrons. This implies that the space-time is de Sitter-like. The polyhedral universe cannot expand from or contract to a point but has minimum edge length  $l_0$ , as does the continuum solution, as we shall see below.

So far we have worked with Euclidean time. To discuss the evolution of space-time we move to the Minkowskian signature by Wick rotation. This can be done in Eqs. (4.3) and (4.4) simply by letting  $\dot{l}^2, \ddot{l} \rightarrow -\dot{l}^2, -\ddot{l}$ . We thus obtain

$$2\pi - q \arccos \frac{\dot{l}^2 - 4 \cos \frac{2\pi}{p}}{4 + \dot{l}^2} = \frac{q\Lambda}{2} \frac{l^2 \cos \frac{\pi}{p}}{\sqrt{4 \sin^2 \frac{\pi}{p} + \dot{l}^2}}, \quad (4.6)$$

$$\frac{\ddot{l}}{4 + \dot{l}^2} = \frac{\Lambda}{4} l \left[ 1 - \frac{l\ddot{l}}{2(4 \sin^2 \frac{\pi}{p} + \dot{l}^2)} \right]. \quad (4.7)$$

We can read off from the evolution equation that the acceleration  $\ddot{l}$  is always positive. Hence the universe expands as the continuum solution at the beginning for the initial conditions (4.5). The expansion, however, becomes much more rapid than the continuum solution as  $t$  gets large, as we shall see in the next section.

## 5 Numerical solution

The Hamiltonian constraint (4.6) can be solved numerically. It is convenient to use the continuum limit of the dihedral angle  $\theta_i$ . Let us denote it by  $\theta$ ; then  $l$  and  $\dot{l}$  can be expressed as

$$\dot{l}^2 = 4 \sin^2 \frac{\pi}{p} \left( \cot^2 \frac{\pi}{p} \cot^2 \frac{\theta}{2} - 1 \right), \quad (5.1)$$

$$l^2 = \frac{4}{q\Lambda} (2\pi - q\theta) \cot \frac{\theta}{2}. \quad (5.2)$$

The first of these can be obtained directly from Eq. (3.5). The second can be derived from the Hamiltonian constraint (4.3) by replacing  $\dot{l}^2$  with Eq. (5.1). Since  $\dot{l}^2 \geq 0$ , the dihedral angle satisfies  $0 \leq \theta \leq \theta_p$ , where  $\theta_p = \frac{(p-2)\pi}{p}$  stands for the interior angle of a  $p$ -sided regular polygon. The edge length is a decreasing function of  $\theta$  satisfying  $l = l_0$  for  $\theta = \theta_p$ . As  $\theta \rightarrow 0$ , it approaches infinity.

Eliminating the edge length from Eqs. (5.1) and (5.2), we obtain the differential equation describing the time development of  $\theta$  as

$$\dot{\theta} = \mp \frac{2\sqrt{2q\Lambda(2\pi - q\theta) \sin \theta \sin \frac{\theta_p + \theta}{2} \sin \frac{\theta_p - \theta}{2}}}{2\pi - q(\theta - \sin \theta)}, \quad (5.3)$$

where the upper (lower) sign corresponds to an expanding (contracting) universe. As can be seen from Eqs. (5.2) and (5.3), the polyhedral universe expands to infinity at  $t = t_{p,q}$  given by

$$t_{p,q} = \int_0^{\theta_p} d\theta \frac{2\pi - q(\theta - \sin \theta)}{2\sqrt{2q\Lambda(2\pi - q\theta) \sin \theta \sin \frac{\theta_p + \theta}{2} \sin \frac{\theta_p - \theta}{2}}}. \quad (5.4)$$

In what follows we focus our attention on the expanding universe. Solving Eq. (5.3) numerically for the initial condition

$$\theta(0) = \theta_p - \epsilon, \quad (5.5)$$

we can find the evolution of the polyhedral universe, where we have introduced the positive infinitesimal  $\epsilon$  to avoid the trivial solution  $\theta(t) = \theta_p$ . It is also possible to solve numerically the evolution equation (4.7) with the initial condition (4.5). We shall use the latter approach in obtaining numerical solutions for the geodesic dome universe, where the edge lengths cannot be parametrized by a single dihedral angle.

To compare with the continuum theory we must introduce an analog of the scale factor  $a(t)$ . In Ref. [10] the authors discussed various definitions for the scale factor in a discretized FLRW universe in four dimensions. The behavior of universe, however, does not depend so much on the definition. Here, we simply define the scale factor of our polyhedral universe  $a_R$  as the radius of the circumsphere of the polyhedron. It is given by

$$a_R(t) = \frac{l(t) \sin \frac{\pi}{q}}{2\sqrt{\sin^2 \frac{\pi}{p} - \cos^2 \frac{\pi}{q}}}. \quad (5.6)$$

The initial scale factor can be easily found as

$$a_R(0) = \sqrt{\frac{\pi \left( \frac{2}{p} + \frac{2}{q} - 1 \right) \tan \frac{\pi}{p}}{\Lambda \left( \sin^2 \frac{\pi}{p} - \cos^2 \frac{\pi}{q} \right)}} \sin \frac{\pi}{q}. \quad (5.7)$$

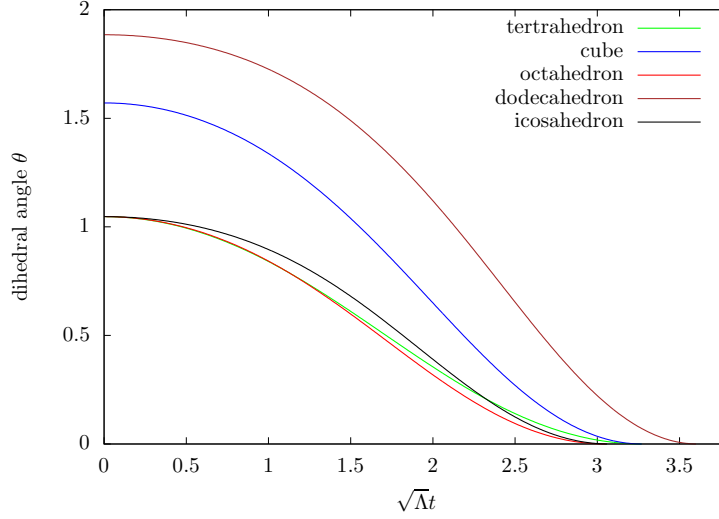


Figure 2: Plots of the dihedral angles of the regular polyhedral models: each plot ends at  $t = t_{p,q}$ .

In Fig. 2 the dihedral angles are plotted for the five types of regular polyhedrons. They are monotone decreasing functions of time and approach zero as  $t \rightarrow t_{p,q}$ . In Fig. 3 we give the plots of the scale factors of the polyhedral universes as functions of time. The broken curve corresponds to the continuum solution. One can see that the polyhedral solutions approximate well the continuum at around  $t = 0$ . This can be understood by noting the fact that the scale factor (5.6) approximately satisfies the Friedmann equation (1.3) when both  $\sqrt{\Lambda}l$  and  $\dot{l}$  are small.

The deviations from the continuum solution, however, get large for  $t > 2/\sqrt{\Lambda}$ . The polyhedral universe expands much faster than the continuum FLRW universe and approaches an infinite size as  $t \rightarrow t_{p,q}$ . In fact, it is easy to see from Eqs. (5.1) and (5.2) that  $a_R(t)$  is approximately given by

$$\sqrt{\Lambda}a_R \approx \frac{c_{p,q}}{\sqrt{\Lambda}(t_{p,q} - t)}, \quad (5.8)$$

where  $c_{p,q}$  is defined by

$$c_{p,q} = \frac{2\pi}{q} \frac{\sec \frac{\pi}{p} \sin \frac{\pi}{q}}{\sqrt{\sin^2 \frac{\pi}{p} - \cos^2 \frac{\pi}{q}}}. \quad (5.9)$$

In Fig. 3 one can see the similarity between the octahedron and icosahedron. This can be understood from  $c_{3,4} \approx c_{3,5}$  and  $t_{3,4} \approx t_{3,5}$ . A similar thing also occurs for the tetrahedron and cube.

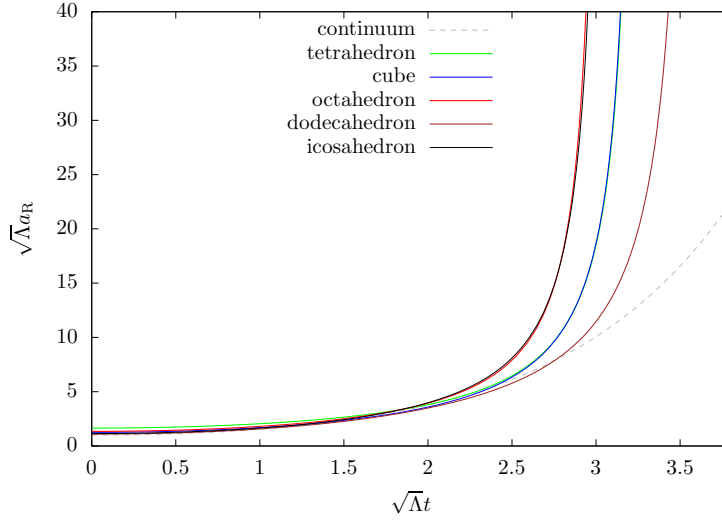


Figure 3: Plots of the scale factors of the regular polyhedral models.

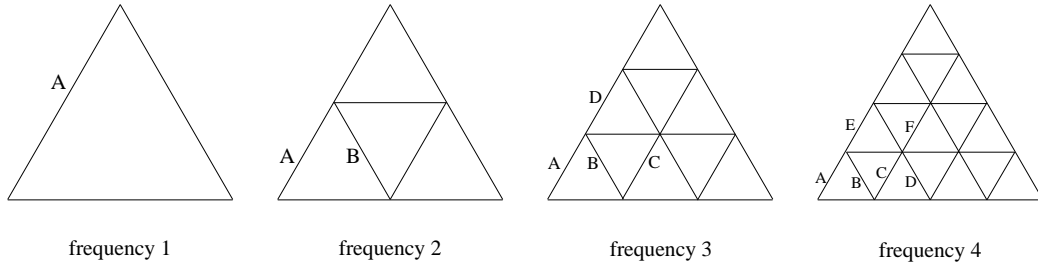


Figure 4: Subdivision of a regular triangle: sides with distinct alphabetical labels are projected onto edges of different lengths in the geodesic dome.

## 6 The geodesic dome and pseudo-regular polyhedral universes

If we cease to stick to regular polyhedrons as the Cauchy surfaces, we can approximate a sphere more precisely. One way to put this into practice is to introduce geodesic domes. As depicted in Fig. 4, each face of a regular icosahedron can be subdivided into  $\nu^2$  similar regular triangles, where  $\nu = 1, 2, 3, \dots$  is the degree of subdivision, called the frequency. A geodesic dome is then obtained by projecting the icosahedron tessellated by the  $20\nu^2$  triangular tiles onto the circumsphere. We show the first four geodesic domes in Fig. 5.

The numbers of vertices, edges, and faces of the geodesic domes are summarized in Table 2. Geodesic domes have only two types of connectors: the five-way connectors corresponding to the vertices of the original icosahedron, and the six-way connectors. Note that the larger the frequency, the more six-way connectors are used, while the number of five-way connectors is always 12. Furthermore, the faces of a geodesic dome are not regular triangles, except for the center triangles appearing for  $\nu \equiv 1, 2 \pmod 3$ . The number of types of edges with

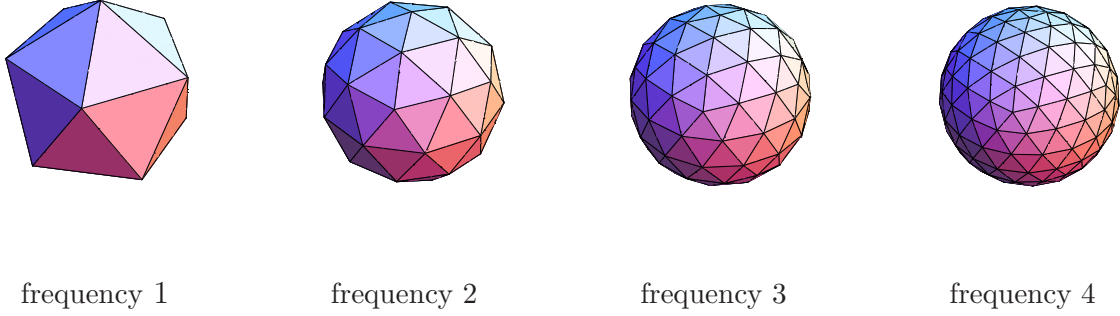


Figure 5: Projection of tessellated icosahedrons onto the circumsphere.

Frequency:		1	2	3	...	$\nu$
$N_2$		20	80	180	...	$20\nu^2$
$N_1$	Type A	30	60	60		
	Type B		60	90		
	Type C			120		
	$\vdots$					
	Total	30	120	270	...	$30\nu^2$
$N_0$	Five-way connectors	12	12	12	...	12
	Six-way connectors	0	30	80	...	$10(\nu^2 - 1)$
	Total	12	42	92	...	$10\nu^2 + 2$

Table 2: Numbers of faces, links, and vertices of geodesic domes.

different lengths is given by

$$M = \begin{cases} \frac{(\nu + 1)^2}{4} & (\nu \text{ odd}), \\ \frac{\nu^2 + 2\nu}{4} & (\nu \text{ even}). \end{cases} \quad (6.1)$$

Fortunately, we can take as  $l_i$  the length of an edge between a five-way connector and a six-way one since any other edge lengths are proportional to  $l_i$ . Furthermore, all the struts connecting two adjacent Cauchy surfaces have the same length  $m_i$  as in the case of the polyhedral universe. The geodesic dome model is then described by a single set of equations, the Hamiltonian constraint and the evolution equation. It is not difficult to carry out the Regge calculus for  $\nu$  small, as we show in the appendix. The number of different types of edges, however, grows roughly quadratically in  $\nu/2$ . This makes the Regge calculus rather cumbersome for large  $\nu$ .

To avoid the complexity of carrying out the Regge calculus for the geodesic dome, we regard it as a pseudo-regular polyhedron of edge length  $l$  and assume that Eqs. (4.6) and (4.7) still hold true. How about the Schläfli symbol  $\{p, q\}$ ? Since all the faces of the geodesic

dome are triangles, we use  $p = 3$ . As for  $q$ , we employ the average number of faces meeting at a vertex. We thus assign the fractional Schläfli symbol for the geodesic dome of frequency  $\nu$  as

$$\{p, q\} = \left\{ 3, \frac{60\nu^2}{10\nu^2 + 2} \right\}. \quad (6.2)$$

This recovers the icosahedron for  $\nu = 1$  and approaches  $\{3, 6\}$  as  $\nu$  gets large, which corresponds to the tessellation of a flat plane with regular triangles. To see how the pseudo-regular polyhedron is close to the geodesic dome, we note that numerically the deviation of the averaged edge length  $\bar{l}$  of the geodesic domes from  $l$  satisfies, for  $\nu \geq 3$ ,

$$\left| \frac{\bar{l} - l}{l} \right| < 0.0013. \quad (6.3)$$

Hence it is legitimate to think of  $l$  as the averaged edge length of the corresponding geodesic dome.

If we introduce the dihedral angle for the pseudo-regular polyhedron universe by Eq. (5.2) as in the regular polyhedron cases and define the scale factor as Eq. (5.6), then the evolution of the universe can be described by Eq. (5.3) with the parameters (6.2). The initial edge length is given by

$$l(0) = \sqrt{\frac{4\sqrt{3}\pi}{\Lambda} \left( \frac{2}{q} - \frac{1}{3} \right)} = \frac{1}{\nu} \sqrt{\frac{4\sqrt{3}\pi}{15\Lambda}}. \quad (6.4)$$

In contrast to the cases of regular polyhedrons, this can be arbitrarily small as  $\nu \rightarrow \infty$ , or equivalently  $q \rightarrow 6$ . The initial scale factor (5.7), however, approaches the value of the continuum theory, as can easily be seen from

$$a_R(0) = 2\sqrt{\frac{\sqrt{3}\pi(\frac{2}{q} - \frac{1}{3})}{\Lambda(3 - 4\cos^2\frac{\pi}{q})}} \sin\frac{\pi}{q} \rightarrow \frac{1}{\sqrt{\Lambda}} \quad (\nu \rightarrow \infty). \quad (6.5)$$

There is no difficulty in numerically integrating (5.3) for fractional  $q$ . We give plots of the dihedral angle in Fig. 6 and the scale factor in Fig. 7 as functions of time for  $\nu \leq 5$ . As mentioned before, the dihedral angle is a monotone decreasing function of time. The era of almost constant dihedral angle for small  $\sqrt{\Lambda}t$  gets longer with the frequency. The time evolution of the dihedral angles becomes slower as we refine the triangulation of the Cauchy surface. The scale factor, however, develops as depicted in Fig. 7 since the ratio of the scale factor to the edge length becomes large with the frequency. One easily sees that the results for the polyhedral universe given in Sect. 4 are improved more and more as  $\nu$  increases.

As mentioned above, the pseudo-regular polyhedron is not the geodesic dome. Readers may wonder to what extent our model reproduces the geodesic dome universe. It is possible to justify our approach by comparing with the results of the Regge calculus for the geodesic

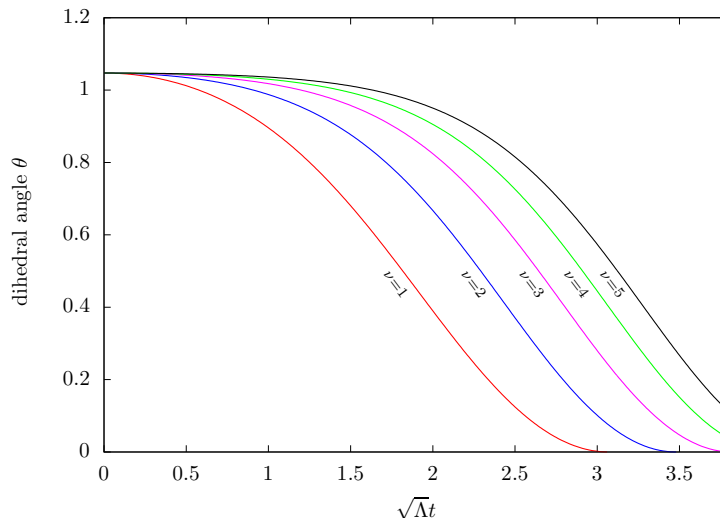


Figure 6: Plots of the dihedral angles of pseudo-regular polyhedral universes for  $\nu \leq 5$ .

dome universe. We have carried this out for  $\nu \leq 5$ . To give readers some feeling for the Regge calculus, the Hamiltonian constraints for the geodesic dome universes with  $\nu = 2$  and  $\nu = 3$  are shown in the appendix. The evolution equations can be obtained by differentiating them with respect to time. We can also read off the initial conditions from the Hamiltonian constraints. It is straightforward to obtain numerical solutions to the evolution equations. The results are plotted in Fig. 7. The plots for the pseudo-regular polyhedrons almost overlap with those for the corresponding geodesic domes. The rates of deviation of the scale factor  $a_R$  for the pseudo-regular polyhedron universe from the scale factor  $a_{gd}$  of the corresponding geodesic dome universe can be found in Fig. 8. We see that the pseudo-regular polyhedron model better approximates the geodesic dome universe as the frequency increases.

Having established the relation with the geodesic dome universe, we can apply the pseudo-regular polyhedron model to the cases where the direct Regge calculus can hardly be practical. In Fig. 9 we give the dihedral angle for  $\nu = 100$ . It approaches a constant solution,

$$\theta(t) \rightarrow \theta_\infty(t) = \frac{\pi}{3}, \quad (6.6)$$

in the infinite frequency limit. Indeed,  $\theta_\infty(t)$  satisfies Eqs. (5.5) and (5.3), as one can verify directly. The scale factor for the pseudo-regular polyhedral universe with  $\nu = 100$  is plotted in Fig. 10. During the era of almost constant dihedral angle the agreement with the continuum scale factor can be seen immediately.

Finally, it can be shown that the scale factor of the pseudo-regular polyhedral universe,

$$a_R(t) = \frac{l(t) \sin \frac{\pi}{q}}{\sqrt{3 - 4 \cos^2 \frac{\pi}{q}}}, \quad (6.7)$$

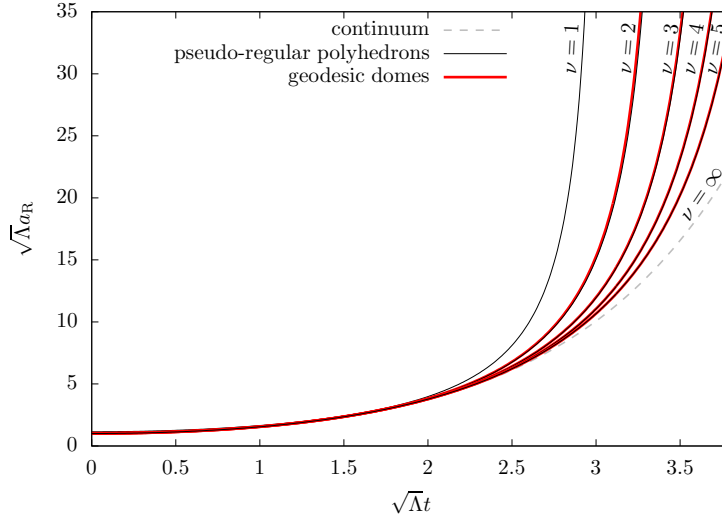


Figure 7: Plots of the scale factors of pseudo-regular polyhedrons and geodesic domes for  $\nu \leq 5$ .

approaches that of the continuum theory in the infinite frequency limit. The easiest way to see this is to come back to Eqs. (4.6) and (4.7). Rewriting them in terms of  $a_R$  and then taking the limit  $q \rightarrow 6$ , we obtain the continuum equations of the scale factor (1.3). This also justifies the approach regarding Eqs. (4.6) and (4.7) as the equations of motion of the discretized FLRW universe.

## 7 Summary and discussions

We have investigated the closed FLRW universe in three dimensions using the CW formalism in Regge calculus. We have given unified expressions applicable to any regular polyhedron as the Cauchy surfaces. We have shown that the Regge equations in the continuum Lorentzian time limit, one corresponding to the Hamiltonian constraint and the other to the evolution equation, describe the evolution of the universe. In spite of the simplest approximations of spheres by regular polyhedrons, the coincidence with the continuum solution is appreciable when the size of the universe is around the minimum, where the nonlinearity of the evolution equation (4.7) can be neglected. The discrepancies, however, become larger and larger with the size of the universe. The polyhedral universe expands much faster than the continuum FLRW universe. This is because the nonlinearity always enhances the acceleration of the universe.

The expansion of the regular polyhedral universe can be slowed down by refining the triangulation of the Cauchy surface. To carry this out systematically we employed geodesic dome models and introduced pseudo-regular polyhedrons. We proposed the pseudo-regular polyhedral universe described by Eqs. (4.6) and (4.7) with the fractional Schläfli symbol (6.2)



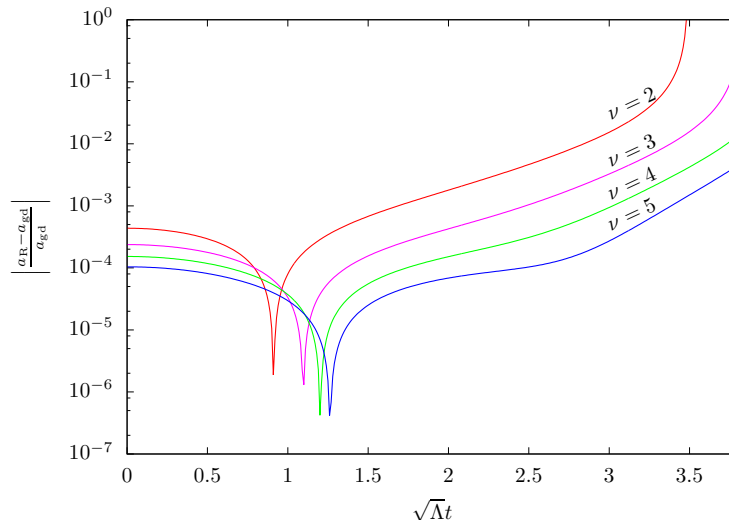


Figure 8: Plots of  $|a_R - a_{gd}|/a_{gd}$  for  $2 \leq \nu \leq 5$ .

as a substitute for geodesic domes. We have shown that our model considerably approximates the geodesic dome universes. As it should be, the continuum solution can be obtained in the infinite frequency limit.

We have considered a closed compact universe. In the continuum theory there is an oscillating solution for a negative cosmological constant, where the Cauchy surface is not compact. Application of our approach to a hyperspherical universe might be interesting. Our concern in this work was the vacuum solution. Hence, the inclusion of matter would be worth investigation. We have worked with three dimensions. It would be of great interest to extend our approach to the four-dimensional FLRW universe.

### Acknowledgments

The authors would like to thank Y. Hyakutake, N. Motoyui, M. Sakaguchi, and S. Tomizawa for useful discussions. This work was supported in part by Grant-in-Aid for Scientific Research Number 24540247 from the Japan Society for the Promotion of Science.

## A Regge calculus for the geodesic domes

In this appendix we give the Hamiltonian constraints for the geodesic dome models of frequencies  $\nu = 2$  and 3. The subdivided faces in Fig. 4 are projected onto the sphere as depicted in Fig. 11. Edges of different lengths are labeled  $A'$ ,  $B'$ ,  $\dots$ . Faces and vertices of different types are denoted  $f_n$  and  $v_m$ , respectively. We choose the length of type  $A'$  edge as  $l_i$ . All other edge lengths can be expressed by  $l_i$  and the angles  $\xi$ ,  $\eta$ , and  $\zeta$ .

To write down the Hamiltonian constraint we need the deficit angle  $\varepsilon_{m,i}^{(s)}$  about the strut

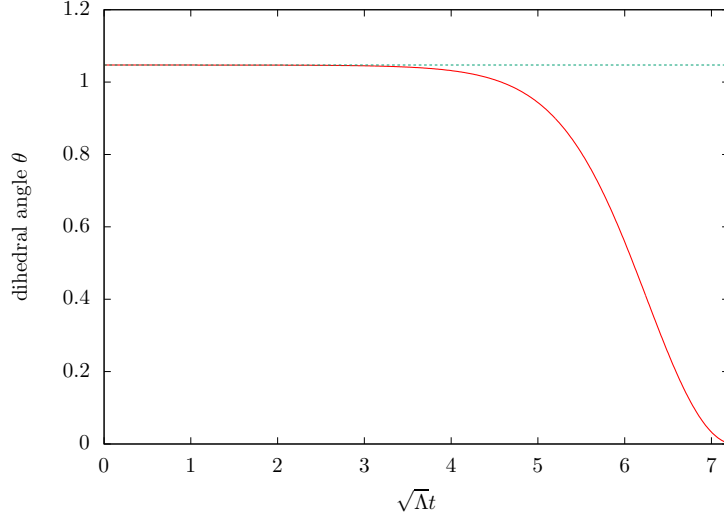


Figure 9: Dihedral angle of the pseudo-regular polyhedron for  $\nu = 100$ . The broken line corresponds to the solution in the infinite frequency limit  $\theta_\infty(t) = \pi/3$ .

$m_i$  at the vertex  $v_m$  and the volume element  $V_{n,i}$  with  $f_n$  as the bottom face. The deficit angles can be expressed by dihedral angles as Eq. (3.4). Since a dihedral angle appearing in  $V_{n,i}$  is uniquely determined by specifying a strut in the volume element, we denote the dihedral angle about the strut  $m_i$  at the vertex  $v_m$  by  $\theta_{m,n,i}$ . Then the deficit angle  $\varepsilon_{m,i}^{(s)}$  is given by

$$\varepsilon_{m,i}^{(s)} = 2\pi - \sum_n \theta_{m,n,i}, \quad (\text{A.1})$$

where the summation must be taken over the indices  $n$  of the volume elements with strut  $m_i$  in common. There are three different types of dihedral angles for  $\nu = 2$  case:  $\theta_{1,1,i}$ ,  $\theta_{2,1,i}$ , and  $\theta_{2,2,i}$ . The number of independent dihedral angles is six for  $\nu = 3$ . Concrete expressions for  $V_{n,i}$  and  $\theta_{m,n,i}$  in terms of  $l_i$  and  $m_i$  can be found by standard geometry.

We are now able to write the Hamiltonian constraints. They are:

$$\nu = 2 : \frac{1}{5}\varepsilon_{1,i}^{(s)} + \frac{1}{2}\varepsilon_{2,i}^{(s)} = \Lambda \left( \frac{\partial V_{1,i}}{\partial m_i} + \frac{1}{3} \frac{\partial V_{2,i}}{\partial m_i} \right), \quad (\text{A.2})$$

$$\nu = 3 : \frac{1}{5}\varepsilon_{1,i}^{(s)} + \varepsilon_{2,i}^{(s)} + \frac{1}{3}\varepsilon_{3,i}^{(s)} = \Lambda \left( \frac{\partial V_{1,i}}{\partial m_i} + \frac{\partial V_{2,i}}{\partial m_i} + \frac{\partial V_{3,i}}{\partial m_i} \right). \quad (\text{A.3})$$

The coefficients in front of the deficit angles and volume elements can be found by counting the number of vertices of type  $v_m$  and the number of volume elements with  $f_n$  as the bottom face.

Taking the limit of continuum time followed by the Wick rotation, we finally obtain, for

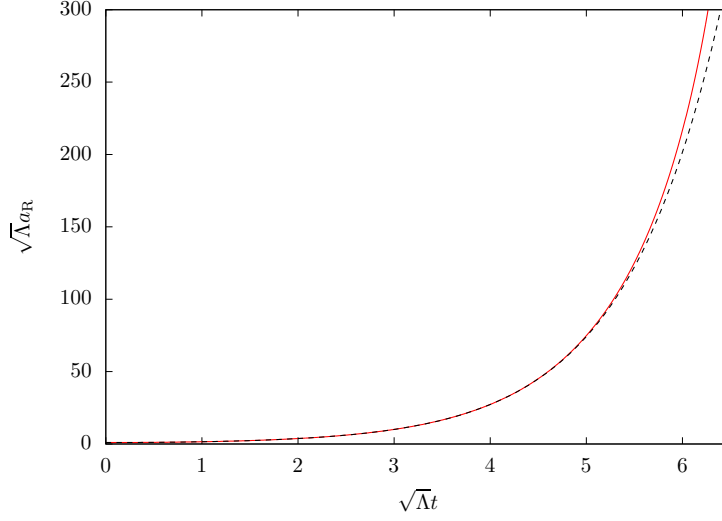


Figure 10: Scale factor of the pseudo-regular polyhedron for  $\nu = 100$ . The broken curve is the scale factor of the continuum theory.

$\nu = 2$ ,

$$\frac{1}{5}\varepsilon_1^{(s)} + \frac{1}{2}\varepsilon_2^{(s)} = \Lambda l^2 \left[ \frac{\sin \xi \cos \frac{\xi}{2}}{\sqrt{4 \cos^2 \frac{\xi}{2} + l^2}} + \frac{\sin^2 \frac{\xi}{2}}{\sqrt{3 + 4l^2 \sin^2 \frac{\xi}{2}}} \right]. \quad (\text{A.4})$$

The deficit angles are given by

$$\varepsilon_1^{(s)} = 2\pi - 5\theta_{1,1}, \quad (\text{A.5})$$

$$\varepsilon_2^{(s)} = 2\pi - 4\theta_{2,1} - 2\theta_{2,2}, \quad (\text{A.6})$$

where the dihedral angles are

$$\theta_{1,1} = \arccos \frac{4 \cos \xi + l^2}{4 + l^2}, \quad (\text{A.7})$$

$$\theta_{2,1} = \arccos \frac{(2 + l^2) \sin \frac{\xi}{2}}{\sqrt{(4 + l^2)(1 + l^2 \sin^2 \frac{\xi}{2})}}, \quad (\text{A.8})$$

$$\theta_{2,2} = \arccos \frac{1 + 2l^2 \sin^2 \frac{\xi}{2}}{2(1 + l^2 \sin^2 \frac{\xi}{2})}. \quad (\text{A.9})$$

For  $\nu = 3$  the deficit angles can be found as

$$\varepsilon_1^{(s)} = 2\pi - 5\theta_{1,1}, \quad (\text{A.10})$$

$$\varepsilon_2^{(s)} = 2\pi - 2(\theta_{2,1} + \theta_{2,2} + \theta_{2,3}), \quad (\text{A.11})$$

$$\varepsilon_3^{(s)} = 2\pi - 3(\theta_{3,2} + \theta_{3,3}), \quad (\text{A.12})$$

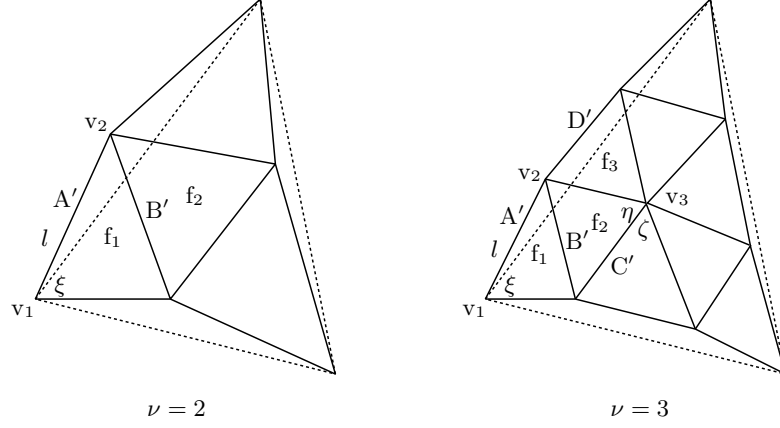


Figure 11: Faces projected onto the sphere.

with

$$\theta_{1,1} = \arccos \frac{4 \cos \xi + \dot{l}^2}{4 + \dot{l}^2}, \quad (\text{A.13})$$

$$\theta_{2,1} = \arccos \frac{(2 + \dot{l}^2) \sin \frac{\xi}{2}}{\sqrt{(4 + \dot{l}^2)(1 + \dot{l}^2 \sin^2 \frac{\xi}{2})}}, \quad (\text{A.14})$$

$$\theta_{2,2} = \arccos \frac{2 \sin^2 \frac{\eta}{2} + \dot{l}^2 \sin^2 \frac{\xi}{2}}{\sqrt{(1 + \dot{l}^2 \sin^2 \frac{\xi}{2})(4 \sin^2 \frac{\eta}{2} + \dot{l}^2 \sin^2 \frac{\xi}{2})}}, \quad (\text{A.15})$$

$$\theta_{2,3} = \arccos \frac{(2 \sin^2 \frac{\eta}{2} + \dot{l}^2 \sin^2 \frac{\xi}{2}) \sin \frac{\zeta}{2}}{\sqrt{(4 \sin^2 \frac{\eta}{2} + \dot{l}^2 \sin^2 \frac{\xi}{2})(\sin^2 \frac{\eta}{2} + \dot{l}^2 \sin^2 \frac{\xi}{2} \sin^2 \frac{\zeta}{2})}}, \quad (\text{A.16})$$

$$\theta_{3,2} = \arccos \frac{4 \cos \eta \sin^2 \frac{\eta}{2} + \dot{l}^2 \sin^2 \frac{\xi}{2}}{4 \sin^2 \frac{\eta}{2} + \dot{l}^2 \sin^2 \frac{\xi}{2}}, \quad (\text{A.17})$$

$$\theta_{3,3} = \arccos \frac{4 \cos \zeta \sin^2 \frac{\eta}{2} + \dot{l}^2 \sin^2 \frac{\xi}{2}}{4 \sin^2 \frac{\eta}{2} + \dot{l}^2 \sin^2 \frac{\xi}{2}}. \quad (\text{A.18})$$

The Hamiltonian constraint is then given by

$$\begin{aligned} & \frac{1}{5} \varepsilon_1^{(s)} + \varepsilon_2^{(s)} + \frac{1}{3} \varepsilon_3^{(s)} \\ &= \Lambda l^2 \left[ \frac{\sin \xi \cos \frac{\xi}{2}}{\sqrt{4 \cos^2 \frac{\xi}{2} + \dot{l}^2}} + \frac{2 \sin^2 \frac{\xi}{2} \cos^2 \frac{\eta}{2}}{\sqrt{\sin^2 \eta + \dot{l}^2 \sin^2 \frac{\xi}{2}}} + \frac{\sin^2 \frac{\xi}{2} \csc \frac{\eta}{2} \sin \zeta \cos \frac{\zeta}{2}}{\sqrt{4 \sin^2 \frac{\eta}{2} \cos^2 \frac{\zeta}{2} + \dot{l}^2 \sin^2 \frac{\xi}{2}}} \right]. \end{aligned} \quad (\text{A.19})$$

The evolution equations can be obtained similarly. They can also be obtained by taking the time derivative of the Hamiltonian constraints. Since they are linear with respect to the second derivative  $\ddot{l}$ , numerical integration is straightforward. In doing this we need initial

conditions. We can assume  $\dot{l}(0) = 0$ . The initial edge length  $l(0)$  can be found from the Hamiltonian constraints. Finally, we define the scale factor  $a_{\text{gd}}$  for the geodesic dome by the radius of the circumsphere. It is nothing but the radius of the circumsphere of the parent icosahedron of the geodesic dome.

## References

- [1] T. Regge, *Il Nuovo Cim.* **19**, 558 (1961).
- [2] C. W. Misner, K. S. Thorne, and J. A. Wheeler, *Gravitation* (Freeman, New York, 1973), Chap. 42.
- [3] F. David, Simplicial quantum gravity and random lattices, in *Gravitation and Quantizations*, eds. B. Julia and J. Zinn-Justin (North-Holland, Amsterdam, 1995), p. 679 [arXiv:hep-th/9303127].
- [4] M. Bañados, C. Teitelboim, and J. Zanelli, *Phys. Rev. Lett.* **69**, 1894 (1992) [arXiv:hep-th/9204099].
- [5] M. Bañados, M. Henneaux, C. Teitelboim, and J. Zanelli, *Phys. Rev. D* **48**, 1506 (1993) [arXiv:gr-qc/9302012].
- [6] S. Carlip, *Class. Quant. Grav.* **22**, R85 (2005) [arXiv:gr-qc/0503022].
- [7] P. A. Collins and R. M. Williams, *Phys. Rev. D* **7**, 965 (1973).
- [8] L. Brewin, *Class. Quant. Grav.* **4**, 899 (1987).
- [9] R. G. Liu and R. M. Williams, *Phys. Rev. D* **93**, 024032 (2016) [arXiv:1501.07614[gr-qc]].
- [10] R. G. Liu and R. M. Williams, *Phys. Rev. D* **93**, 023502 (2016) [arXiv:1502.03000[gr-qc]].
- [11] H. S. M. Coxeter, *Regular Polytopes* (Dover Publications, Inc., New York, 1973).
- [12] W. A. Miller, *Class. Quant. Grav.* **14**, 199 (1997) [arXiv:gr-qc/9708011].
- [13] L. Schläfli, *Quart. J. Pure Appl. Math.* **2**, 269 (1858).
- [14] H. M. Haggard, A. Hedeman, E. Kur, and R. G. Littlejohn, *J. Phys. A: Math. Theor.* **48**, 105203 (2015) [arXiv:1409.7117 [math-ph]].